https://doi.org/10.24199/j.mmv.1973.34.09 9 May 1973

OPALINE SILICAS FROM THE MURRAY RIVER REGION WEST OF WENTWORTH, N.S.W., AUSTRALIA

By E. R. Segnit
CSIRO Division of Mineral Chemistry, Port Melbourne, Australia
J. B. Jones
Geology Department, The University of Adelaide, South Australia
C. A. Anderson
CSIRO Division of Textile Industry, Geelong, Victoria, Australia

A variety of opals and opaline silicas were encountered in the area (Gill, this *Memoir*). They ranged from fine-grained earthy materials to typical glassy opals. There was considerable variation in their manner of occurrence, which reflected differences in the genesis of the various types of opal. The characteristics of the following samples are described in some detail.

1. *Grey-green translucent opal* occurring in the upper layers of the dolomite bed at Devil's Elbow, Nampoo Station. This is a typical, often glassy, opal, uniform in colour. It occurs as concretions and nodules with a white outer skin. In places it passes into the white opal.

2. *White opaque opal* occurring closely associated with the grey-green opal in the upper layers of the dolomite.

3. (a) *White opal breccia* occurs as a band up to 1 m thick above the dolomite at Devil's Elbow, Nampoo Station. This material consists of angular fragments of white opaque opal from 2 cm down to sand size recemented to a massive breccia.

(b) *Brown opal breccia* forms a band up to 0·5 m thick at the base of the dolomite at Devil's Elbow. It consists of closely packed fragments of iron-rich opal cemented to a solid mass.

4. *Brown translucent opal* with dendritic growths. This material occurs in large masses in the clay beds about 0·5 km downstream from the above occurrences. It is a chocolate brown opal, almost transparent in thin chips, and contains small black dendritic growths of what is probably manganese oxide.

5. *Siliceous concretions* from the clayey sand below the Blanchetown Clay at the same locality as 4. These are sandy, very irregular in shape, commonly less than 3 cm in length.

6. *Opal claystone* from a thin band at Kulcurna Station on a former cliff behind the homestead. This is a cohesive, soft but brittle earthy material.

Description of the Opaline Silicas

1. *Grey-green opal*

Microstructure. In thin section this opal is uniform in texture, but between crossed polarizers is seen to be very finely fibrous and birefringent. This structure is typical of a lussatite (opal-CT, Jones and Segnit 1971). A few shadowy structures appear to be relics of original replaced materials, and small cavities are lined with colourless isotropic opal. There are occasional grains of detrital quartz.

Scanning electron micrographs were obtained of freshly broken surfaces, lightly etched with hydrofluoric acid, and coated with gold. A general view of such a surface is shown in Pl. 20, fig. 1, and the central portion of this area is shown in Pl. 20, fig. 2. Despite the glassy nature of this opal, there is an extensive system of very fine pores. The etching has also revealed a very fine substructure of grains or fibres of diameter approximately 1,000 Å; these are the

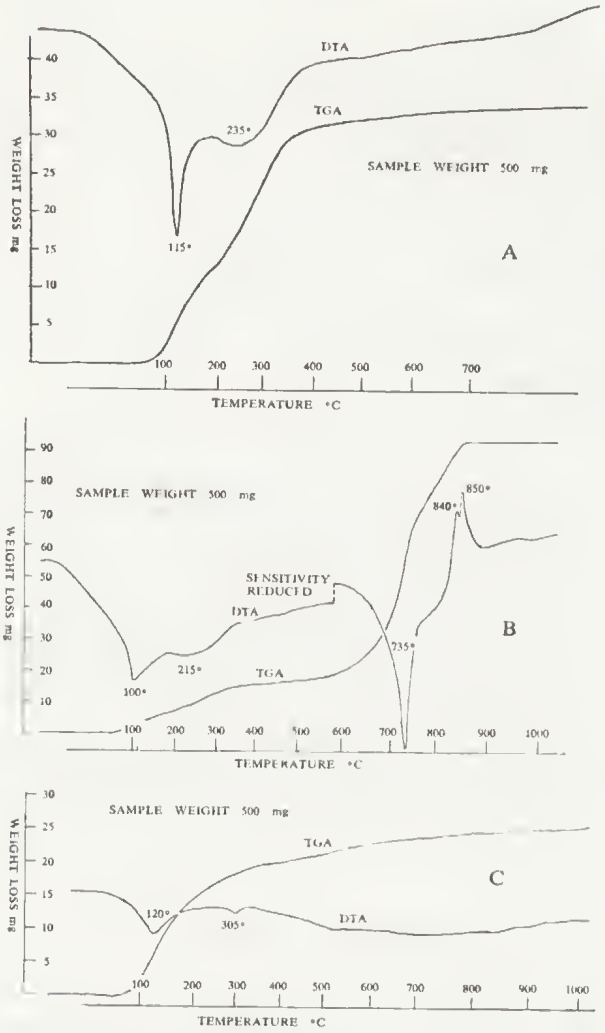

Fig. 1—Differential thermal and thermogravimetric analysis curves of the opaline silicas. A, Grey-green opal. B, Dolomitic opal. C, White opal breccia.

individual crystallites of the disordered cristobalite-tridymite which give rise to the birefringence seen under the optical microscope.

Thermal analysis. Differential thermal analysis and thermogravimetric analysis curves are shown in Fig. 1A. Two low temperature endotherms are recorded, representing two stages of water loss which is also reflected in the weight loss curve. The total weight loss from this sample was 8·45%. The water which was held in capillaries open to the atmosphere boiled off sharply, giving rise to the peak at 115°C. The second, broader peak at 235°C probably represents water which was held in closed micropores; diffusion from these pores would have been more gradual, the diffusion rate reaching a maximum at the temperature indicated.

X-ray diffraction. The X-ray diffraction pattern of this opal (Fig. 2A) shows that it is an opal-CT with a rather high degree of disorder.

2. *White opaque opal*

Microstructure. Microscopic examination showed it to be a very fine-grained, intimate mixture of a carbonate mineral and opaline silica. The particle size of the carbonate mineral was of the order of one micron.

Scanning electron micrographs were made of fracture surfaces lightly etched with hydrochloric acid. Pl. 20, fig. 3 shows a general view of the structure; Pl. 20, fig. 4 shows the central part at a higher magnification. The structure appears to be that of a honeycomb-like network of opaline silica surrounding the grains of the carbonate mineral. Etching with acid has partly dissolved many of the carbonate grains, leaving fragments occupying the cavities.

Thermal analysis. The DTA and TGA curves of this sample are shown in Fig. 1B. These are a combination of the curves for opaline silica and dolomite up to 800°C. The double endotherm at low temperature shows that the opaline silica is of the same type as the grey-green opal. The strong sharp endotherm at 735°C is characteristic of the breakdown and loss of carbon dioxide from the magnesium carbonate component of dolomite. This is followed by two sharp exotherms caused by the reaction of the opaline silica with lime and magnesia to form diopside. The remaining carbon dioxide is lost during this reaction, as is indicated in the TGA curve.

X-ray diffraction. The diffraction pattern in Fig. 2B shows that the white opal is a mixture of opaline silica similar to that of the grey-green opal, and dolomite.

3a. *White opal breccia*

Microstructure. In thin section the white opal particles are rather opaque and show evidence of extensive microcracking. In between the large fragments there is a mixture of small opal grains and quartz grains, with fragments of a

micaceous clay mineral. These are cemented together by transparent colourless opal which shows marked birefringence, and is thus probably opal-CT.

The morphology shown by the scanning electron microscope seems to be that of distorted hollow sub-spherical particles about two microns in diameter packed together in an irregular manner (Pl. 21, fig. 1). The fracture surfaces of these particles show very smooth relief, suggesting that the discrete particles of the former gel were very small, probably less than 200-300 Å. The inner and outer surfaces of the hollow particles show evidence of spheres of the order of 0·2-0·5 microns diameter. These are also occasionally seen on the surfaces of larger cavities (Pl. 21, fig. 2).

Thermal analysis. On drying at 110°C, the loss in weight was 2·43%; on ignition, the additional loss was 3·19%. After evaporation and ignition with hydrofluoric and sulphuric acids the residue was 2·92%, giving a silica content of 91·46%.

The DTA and TGA curves are recorded in Fig. 1C. There is a steady weight loss on heating due to the loss of water from the opal; the DTA curve shows a corresponding weak endotherm, which is common for opal-A. A peak occurs at 125° corresponding to the loss of the physically adsorbed water, followed by a weaker broad endotherm centred on 180°C. A double endotherm of this shape is characteristic of most of the opals, whether opal-A or opal-CT, collected from this area.

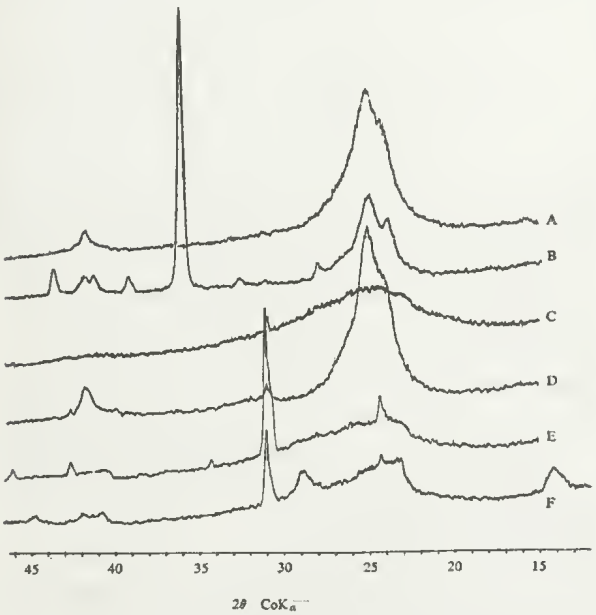

Fig. 2—X-ray diffraction patterns of opaline silicas. A, Grey-green opal. B, Dolomitic opal. C, White opal breccia. D, Brown translucent opal. E, Siliceous concretions. F, Opal claystone.

X-ray diffraction. The X-ray pattern of this material shows no sharp peaks apart from a small peak at 3·34 Å caused by the presence of quartz. The broad hump centred on 4 A (Fig. 2C) is characteristic of the highly disordered form opal-A.

3b. *Brown opal breccia*

The brown opal breccia differs from the white in that it is opal-CT, though poorly ordered in structure. One of its more interesting features is the presence of frequent vugs, the surfaces of which can be seen under the binocular microscope to be coated with minute botryoidal growths. Scanning electron micrographs of the surfaces of the growths show that they are of two types. Some are composed of small crystals of quartz (Pl. 21, fig. 3), whilst others are composed of aggregates of minute crystallites of opal-CT (Pl. 21, fig. 4).

4. *Brown translucent opal*

Microstructure. In thin section this opal is very weakly birefringent, apart from occasional bands and patches. The structure appears to be that of a very finely crystalline opal-CT. Detrital quartz grains are commonly included, and dendritic growths of black to brown oxide, probably manganese, are characteristic (Pl. 23, fig. 1). The latter material has entered and been deposited along fine cracks; in places, the oxide has diffused through the opal near the dendrite, staining it brown. The quartz grains are fairly uniform in size, of the order of 0·5 mm diameter. Shadowy structures seem to be related to a pre-existing grain structure, and very small vugs are concentrically filled with colourless opal.

Scanning electron microscopy of a lightly etched sample shows a smooth surface texture with very small irregular pores (Pl. 22, g. 1).

The surface is even smoother around the borders of vugs (Pl. 22, fig. 2), which themselves appear to represent the growth fronts of the opal-CT. The vug surfaces are comprised of spherulitic masses, the surfaces of which are composed of minute platy crystallites of opal-CT (Pl. 22, fig. 3). These vugs probably correspond to those surrounded by transparent opal as seen in the optical microscope.

Thermal analysis. The DTA and TGA curves of this opal bear a family resmblance to those of the grey-green and white opals (Fig. 3A). A broad double endotherm is caused by loss of water, although the second is much less pronounced. The total weight loss is somewhat higher; loss at 110°C was 5·48%, and loss above this temperature 5·10%.

X-ray diffraction. The X-ray pattern of this opal is almost identical to that of the grey-green material (Fig. 2D). It is an opal-CT with a rather low degree of order. The presence of quartz is also indicated.

5. *Siliceous concretions*

Microstructure. The main feature of the concretions is a fine-grained clay mineral which tends to form pellets, which themselves are cemented together by further clay, and ultimately a colourles opalinc silica (Pl. 23, fig. 2). The latter occurs as thin veinlets between masses of clay, or in discrete areas. Quartz grains are frequent adventitious inclusions which are cemented into the mass by both the clay and the opal.

Scanning electron micrographs of opal areas showe a highly porous structure (Pl. 24, figs. 1-2), with some pores containing botryoidal growth surfaces. A group of such spherical growths is shown in more detail in Pl. 24, fig. 3. The surface of these growths is not perfectly smooth, but is composed of much smaller grokth units (Pl. 24, fig. 4). It is not clear as to whether these are aggregates of spherical particles of silica of the order of 0·1 μm diameter, or whether they are the exposed ends of crystallites growing radially from the centre of the large growths.

Thermal analysis. The composition of random samples is variable owing to the concretionary

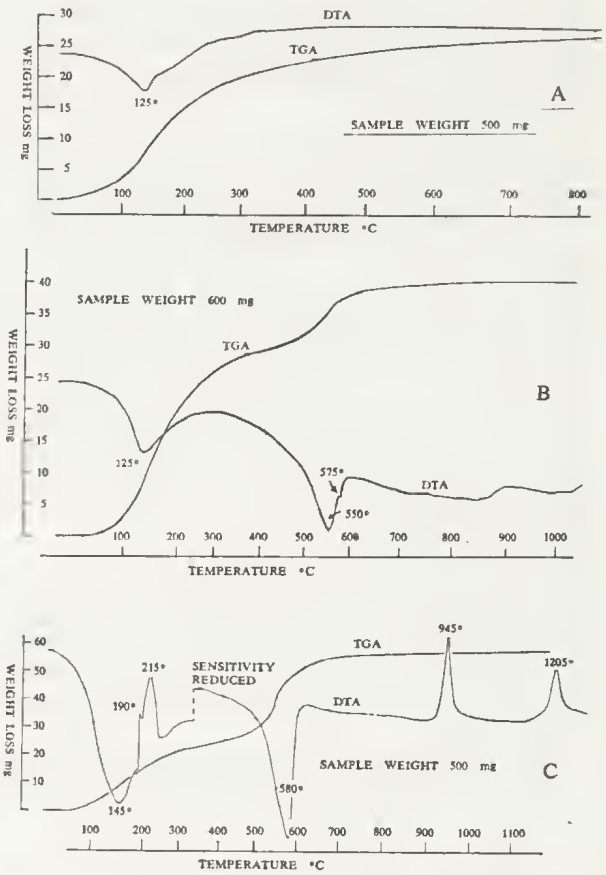

Fig. 3—Differential thermal and thermogravimetric analysis curves of the opaline silicas. A, Brown translucent opal. B, Siliceous concretions. C, Opal claystone.

nature of this material. The DTA and TGA curves (Fig. 3B) are representative of the material, and show the characteristic water-loss endotherm centred on 125°C, followed by the dehydroxylation endotherm of the mica-like clay mineral at 550°C. Superimposed on the side of the latter endotherm is a tiny exothermic peak caused by the $\alpha \rightarrow \beta$ inversion of the quartz in the sample. The TGA curve shows the two stage weight loss from the silica and the clay mineral; the total loss was 6·5% by weight of the original sample.

X-ray diffraction. Fig. 2E shows that the concretions are composed of near amorphous silica, a small amount of quartz, and a poorly ordered illitic clay mineral.

6. *Opal claystone*

Microstructure. This material is very porous,

and consists of a very fine-grained, apparently isotropic clay mineral intimately mixed with an abundance of opaline silica of organic origin. The relics mostly have a spicular habit, sometimes tapering, and frequently with an axial hole (Pl. 25, fig. 1).

The scanning electron micrographs chiefly show an irregular powdery aggregate of clay and silica particles which tend to coat and obscure the organic remains. An example of the spicules which occasionally protrude from the broken surface is in shown in Pl. 25, figs. 2-3.

Thermal analysis. Loss of water at 110°C was 2·86%, and the additional loss on ignition was 8·95%. After evaporation with hydrofluoric and sulphuric acids and ignition, the residue was found to be 18·38%, giving a silica content of 69·81%. Assuming the clay mineral to have the composition $Al_2Si_2O_5(OH)_4$, the mineral composition of the opal claystone is approximately 46% metahalloysite, 54% opal, and the composition of the opal itself is approximately 90% SiO_2, 10% H_2O.

The DTA curve of this material shows some unusual features (Fig. 3C). The broad peak at 145°C represents loss of physically adsorbed water from both the silica and the clay mineral components. Superimposed on, or closely following this, are two exotherms. These occur at approximately 190° and 215°C. These can be assigned to the low temperature oxidation of organic material in the sample. Mr J. D. Saxby and Dr D. J. Swaine of the CSIRO Division of Mineralogy were able to extract and analyse the organic material, which they found to be composed of approximately one-third n-alkanes similar to a light petroleum fraction, with the remainder being a complex mixture of polar compounds. It is not at present known whether this organic material is indigenous, or whether it is contamination from nearby habitation.

At higher temperatures there occur the dehydroxylation endotherm at 580°C of the metahalloysite, and the exotherm caused by the collapse of the layer structure at 945°C. The final broad exotherm at 1,205°C is caused by the recrystallization of the residue of the metahalloysite to cristobalite.

X-ray diffraction. The X-ray pattern of the opal claystone (Fig. 2F) indicates that it is composed of a disordered kaolinitic mineral, probably metahalloysite. The presence of the opaline silica is not clearly shown, owing to its essentially amorphous nature; the broad hump in the region of 4 Å tends to be obscured by the prism reflection of the clay mineral. The silica is present in the form of opal-A. A small amount of quartz is also present. On firing to 1,200°C, the diffraction pattern of the sample becomes that of a well ordered cristobalite.

Discussion

The amount and varieties of opaline silicas occurring in this area reflects the magnitude of movement of silica in solution and as a colloid, and its subsequent deposition. All types except that in the opal claystone were almost certainly deposited during interlacustrine conditions and show evidence of variation in the environments of deposition which in part resulted in differences in the morphologies of the opals.

The opal claystone represents the concomitant accumulation of clay and biogenic silica under quiescent lacustrine conditions. The highly disordered nature of the structure of the clay mineral suggests that it may have been formed in situ from the flocculation of colloidal silica and alumina, rather than being brought in as a fine-grained sediment. This accords with the biogenic silica content, as rates of accumulation of both phases must have been quite slow. This type of material could be a source of supply of relatively soluble silica for subsequent solution, transportation and deposition. Such silica, if widely dispersed even in small amounts in the lake sediments, could be one of the primary sources of the silica of the opaline formations.

The main secondary accumulations of silica are those forming massive and nodular opal. These appear to have been formed probably during drier interlacustrine conditions after the deposition of the sediments in which they are contained. Direct evidence of opalization during the lacustrine era is given by the opal breccias. The white opal-A for example was originally deposited as a near-amorphous silica gel. The structure shown in Pl. ??, fig. 1 suggests very rapid flocculation of a sol on mixing

with electrolyte particles, either solid or in solution. Later drying and hardening was accompanied by extensive cracking, allowing the broken material to be redistributed and recemented with detrital quartz as a local facies of the sediments.

The massive and nodular opals occur both in the dolomite and in the clay beds. The nodular opal in the dolomite was formed mainly near the top of the bed, with subsidiary layers near the base. The silica was probably introduced as a sol moving downwards from the surface drainage during an interlacustrine period. Such a sol would tend to be close to neutral or slightly acid in nature (pH 6-7). Contact with the finely crystalline porous dolomite could raise the concentration of electrolytes quite rapidly and cause flocculation of the silica, which could then accumulate by a filtration process in the intergranular pores around the dolomite crystallites (Pl. 20, figs. 3-4). Further solution of dolomite would allow more silica to accumulate until finally complete replacement occurred. The silica of the sol may already have been crystalline (disordered cristobalite-tridymite), but in any case conditions in the gel were such that crystallite growth of opal-CT occurred (Jones and Segnit 1972) resulting in an opal composed of minute crystallites as seen in Pl. 20, fig. 2.

The major opal-CT formations are nodular to massive in the clay beds. Drying of clay during interlacustrine periods could create cavities in which opal and other materials could accumulate under the appropriate conditions. Sols or solutions of silica could thus percolate through the clay. Gypsum and other salts are common in these clay beds, suggesting that an increase in electrolyte concentration may have caused the flocculation of the silica sol. The formation of crystallites such as those of Pl. 21, fig. 3 represent the final stage in the depositional process in a nodule. These discrete crystallites probably grew more slowly from residual silica solutions derived from the gel, the silica being deposited on crystalline nuclei on the surfaces of vugs as the material slowly dried.

Massive or nodular opal is not found in the sandy beds. The rapid passage of water through these beds with the leaching of electrolytes would result in a less favourable environment for the deposition of opal from descending sols or solutions. The opal represented by sample 5 appears to have a different type of origin. Small amounts of opal-A have in this case been deposited in the sandy beds, together with poorly crystallized clay mineral, around fine plant roots. The clay and the opal may have formed together from the precipitation of colloidal silica and alumina; the formation of an illitic rather than a kaolinitic mineral would have been favoured by the high silica:alumina ratio. The silica may have been derived in part from the remains of overlaying plant material, the root system acting as a pathway for water slowly percolating through the clayey sand.

Since the formation of the opal, weathering processes have etched the surfaces of nodules, sometimes to a depth of several mm. In some cases nodules have been later broken, and a thinner layer of etching can be seen on the younger surface so formed.

References

Jones, J. B. and Segnit, E. R., 1971. The nature of opal 1. Nomenclature and constituent phases. *J. geol. Soc. Aust.* 18: 57-68.

————, 1972. Genesis of cristobalite and tridymite at low temperatures. *J. geol. Soc. Aust.* 18: 419-422.

Explanation of Plates

Plate 20

Figs. 1-2—Scanning electron micrographs of the grey-green opal (lightly etched with HF) from top of dolomite bed, Nampoo Station.
1. General morphology.
2. Crystallite structure of the opal-CT.

Figs. 3-4—Scanning electron micographs of dolomitic opal (lightly etched with HCl) from dolomite bed, Nampoo Station.
3. Honeycomb-like structure with many holes still containing dolomite particles.
4. Detail of central part of 3.

Plate 21

Figs. 1-2—Scanning electron micrographs of the white opal breccia (opal-A) from above dolomite, Nampoo Station.
1. Floc-like structures of the body of the opal.
2. Surface cavity showing aggregates of small silica particles.

Figs. 3-4—Scanning electron micrographs of the crystalline structures in vugs of the brown opal

breccia from the base of the dolomite, Nampoo Station.
3. Crystals of quartz coating surface of vug.
4. Aggregate of crystals of opal-CT forming walls of another vug.

PLATE 22

Figs. 1-3—Scanning electron micrographs of brown translucent opal from Nampoo Station.
1. Lightly etched fracture surface.
2. Final growth surfaces in a vug.
3. Detail of opal-CT crystallites in vug.

PLATE 23

Fig. 1—Photomicrograph of the brown translucent opal from Nampoo Station, showing clear quartz grains and dendritic growths of manganese oxide.

Fig. 2—Photomicrograph of siliceous concretion showing quartz grains, clay pellet structure, and interstitial patches of opaline silica.

PLATE 24

Figs. 1-4—Scanning electron micrographs of a siliceous concretion.
1. General view of an opaline area.
2. Detail of structure of an opaline area.
3. Group of spherical growths in cavity.
4. Detail of surface of spherical growths.

PLATE 25

Fig. 1—Photomicrograph of opal claystone from Kulcurna Station showing the presence of abundant biogenic silica.

Figs. 2-3—Scanning electron micrographs of the opal claystone.
1. Fracture surface showing a protruding sponge spicule.
2. Detail of fracture surface of spicule.

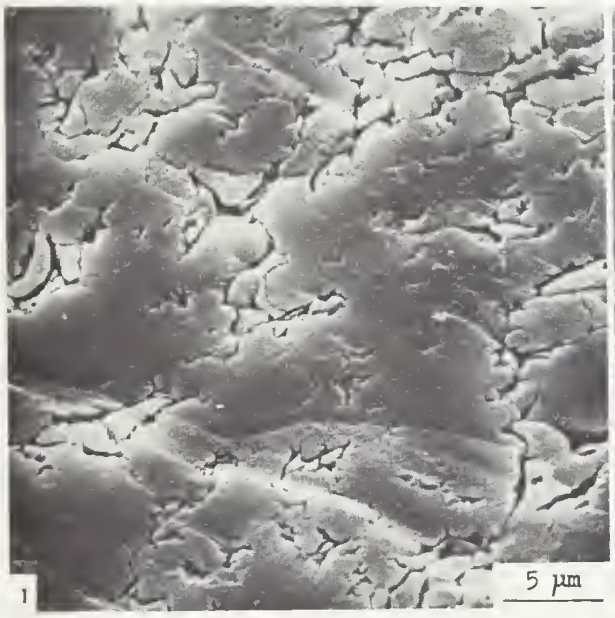
1
5 µm

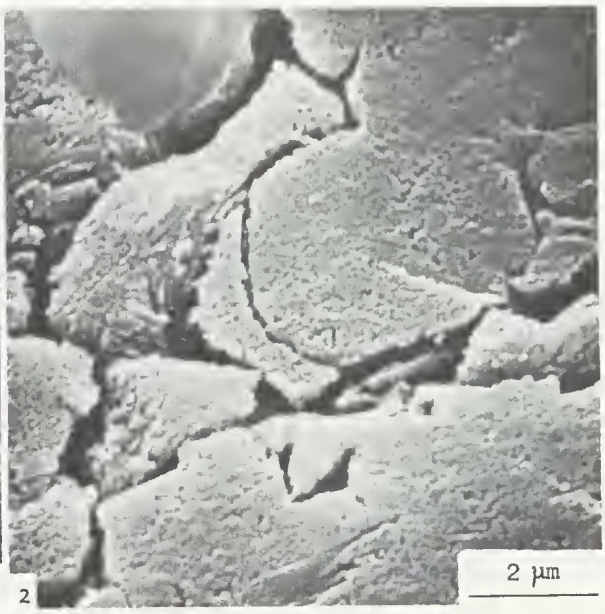
2
2 µm

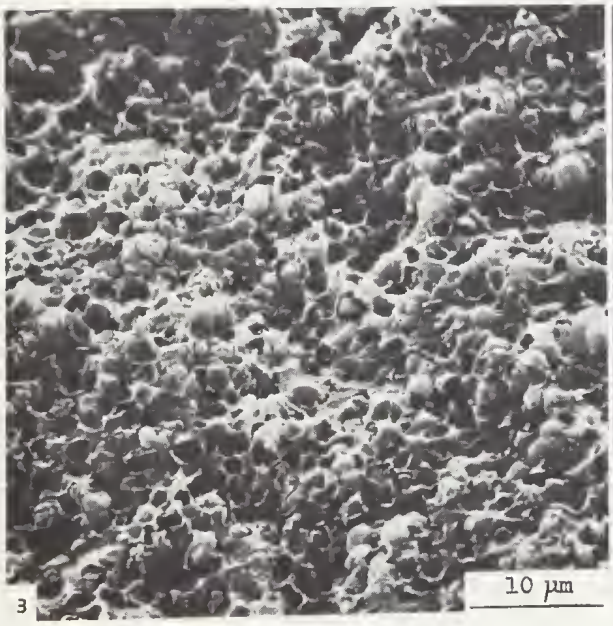
3
10 µm

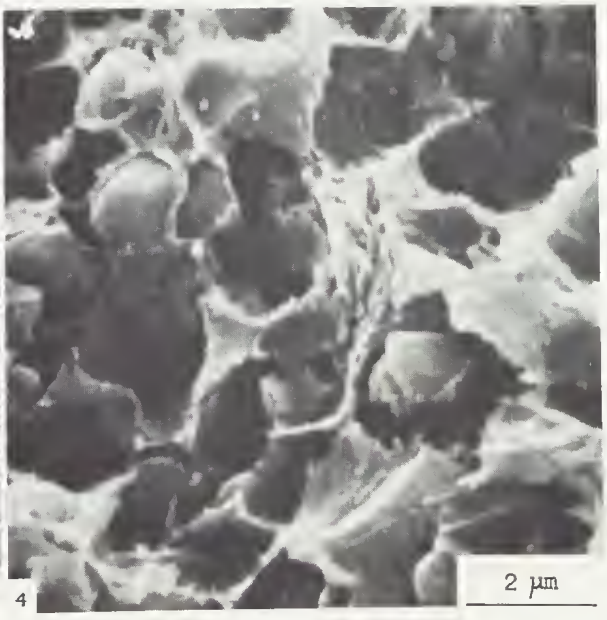
4
2 µm

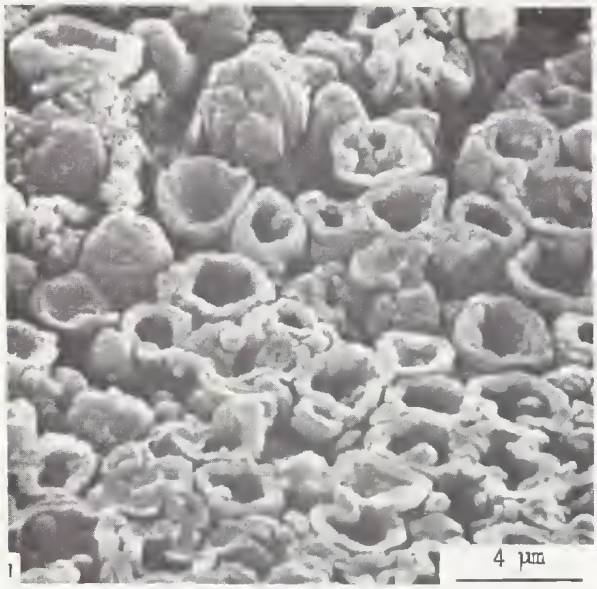

1

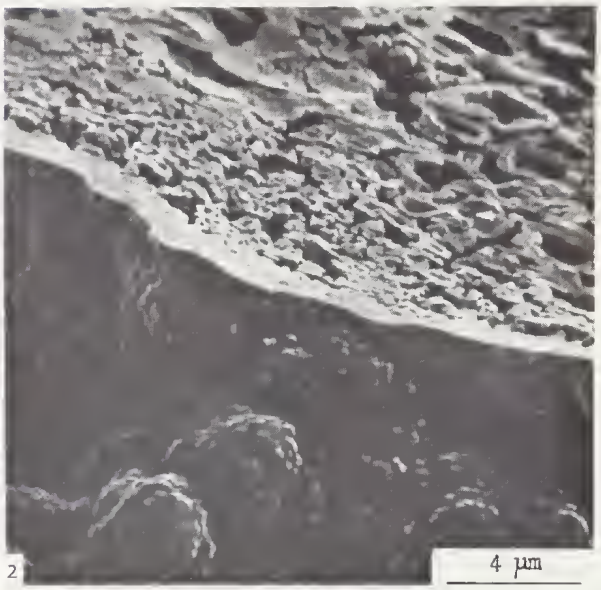

2

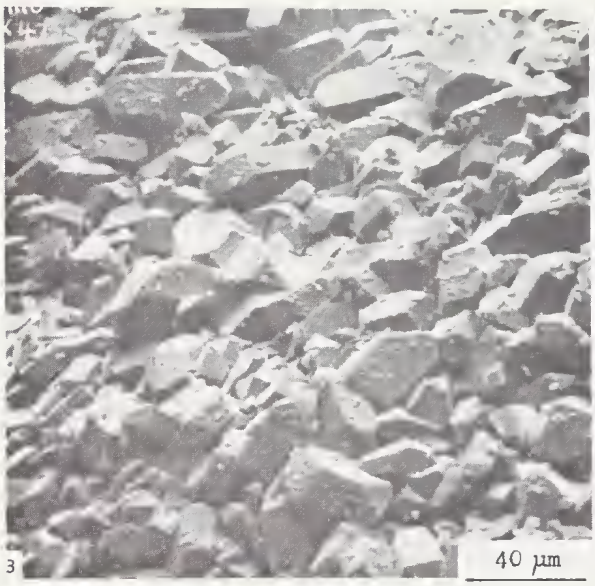

3

4

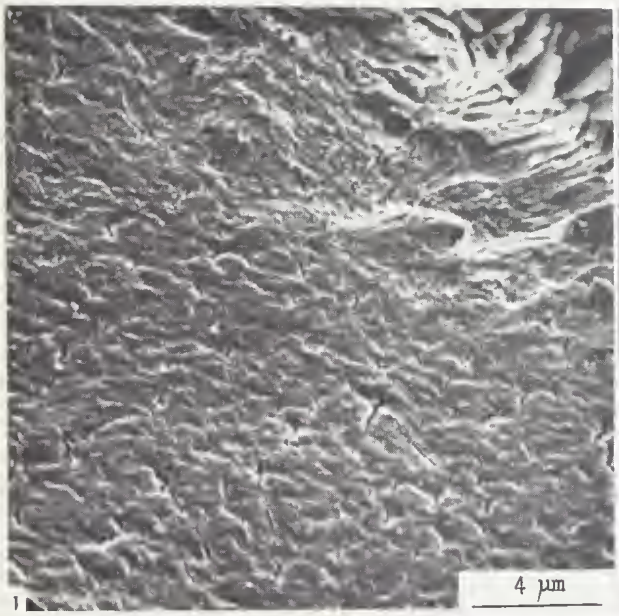

1

2

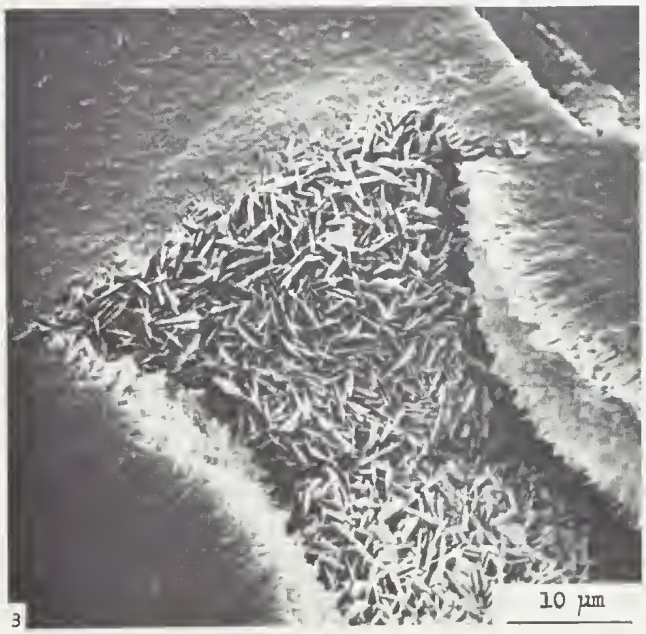

3

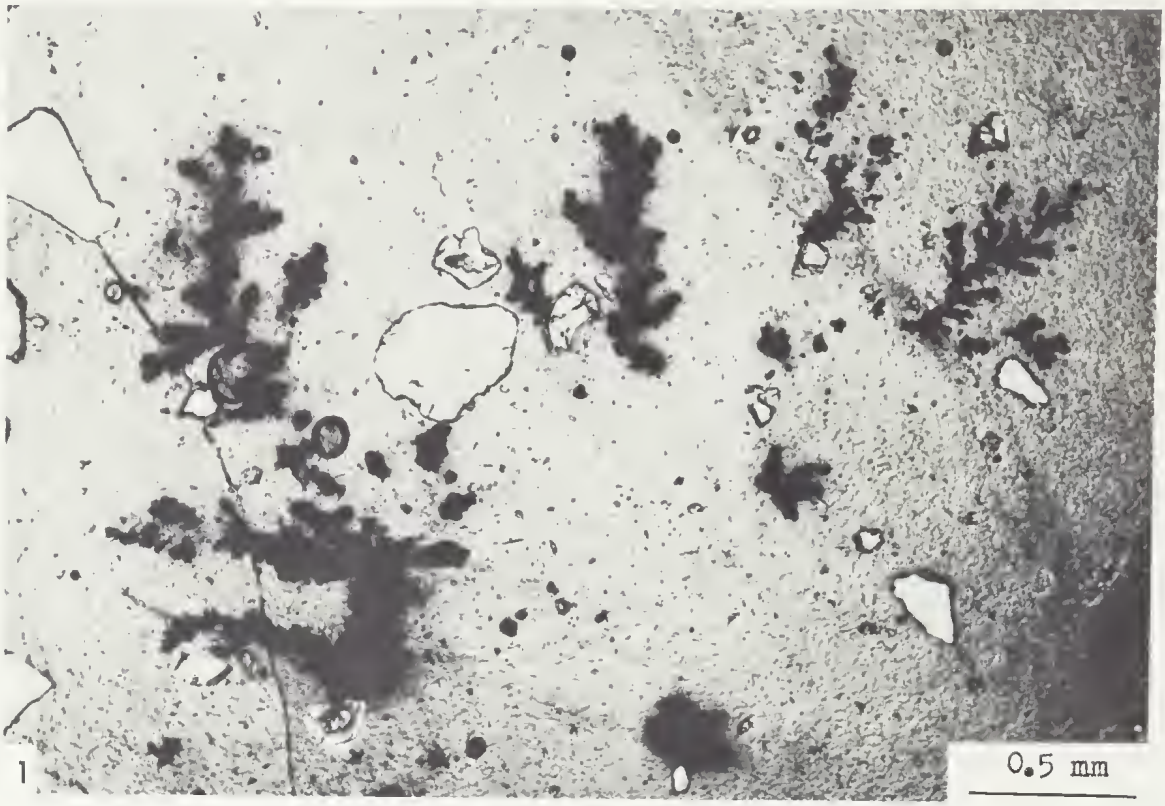
1
0.5 mm

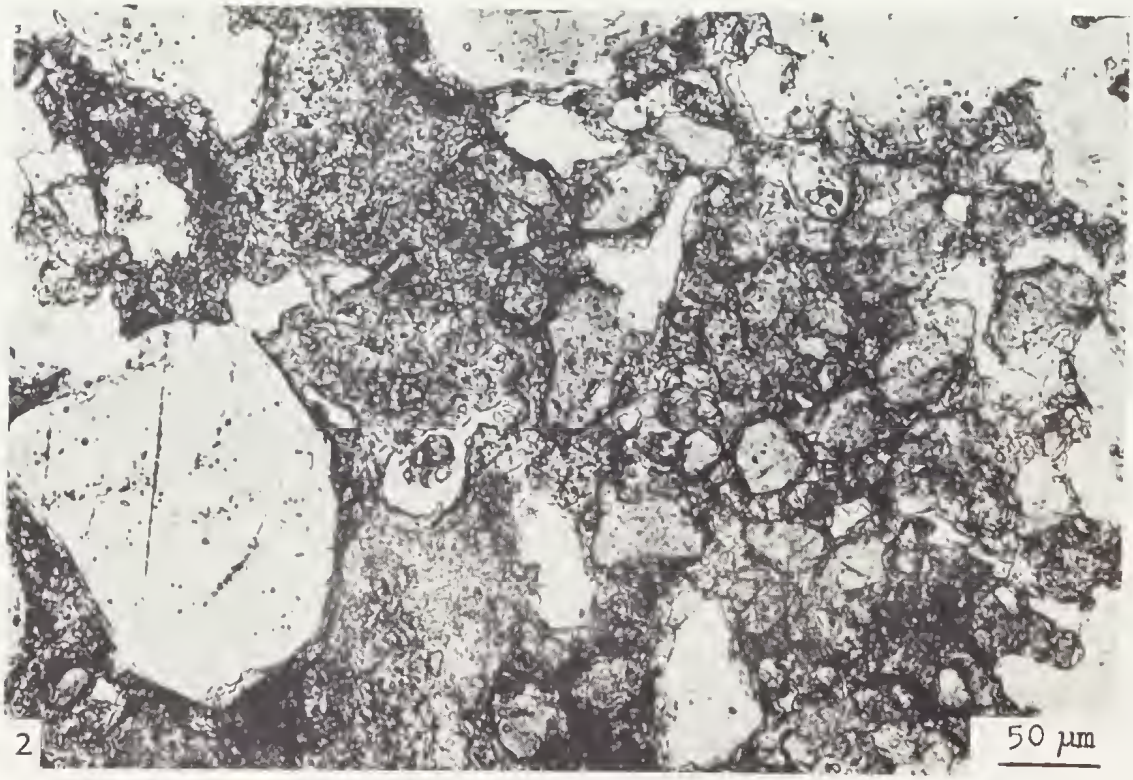
2
50 µm

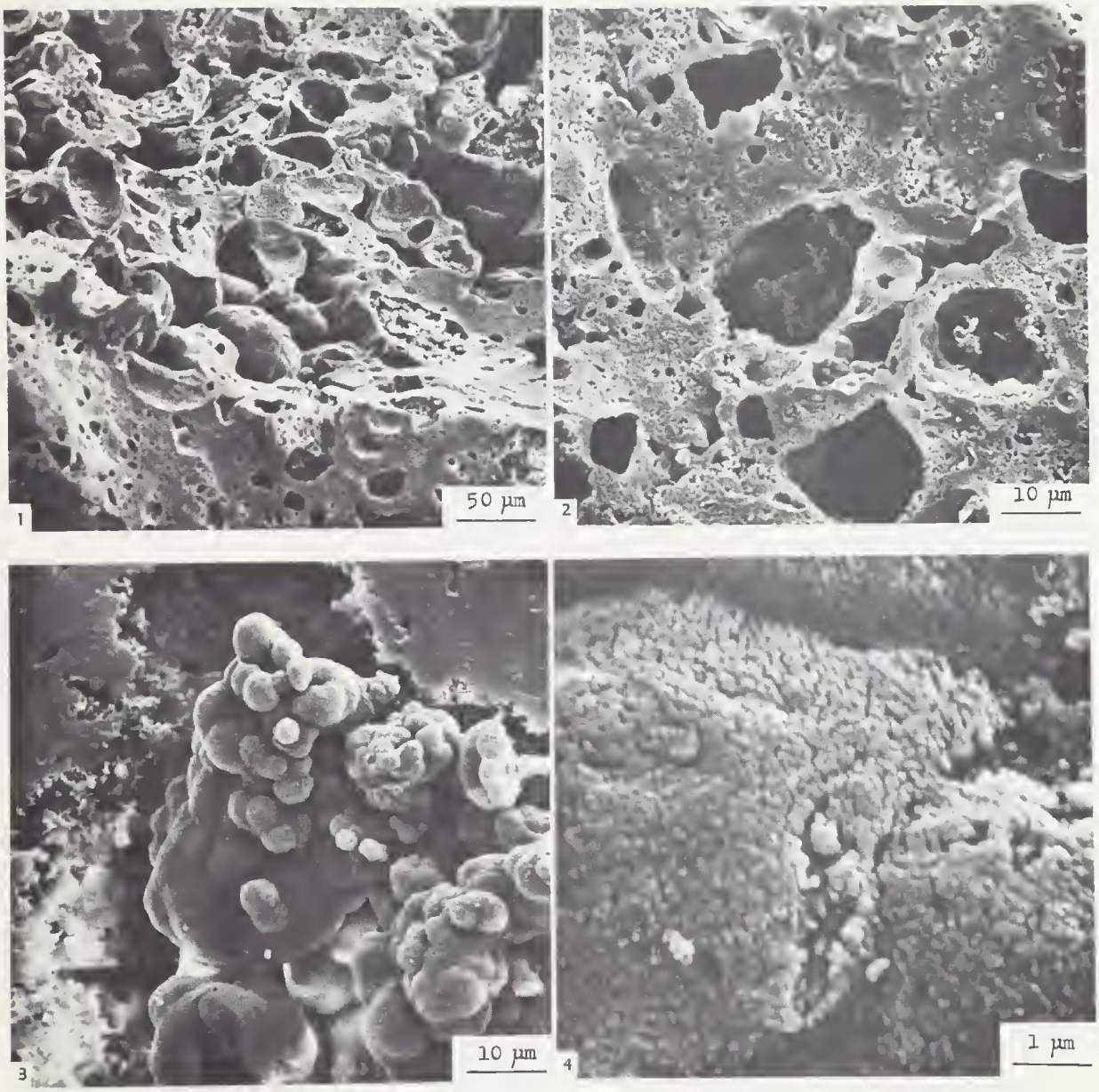
1
50 µm
2
10 µm
3
10 µm
4
1 µm

1

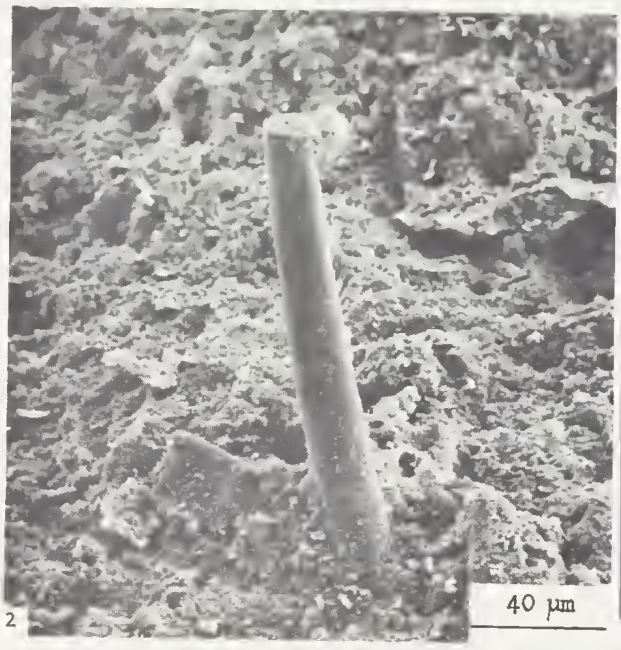

2

3